Lead-germanate glasses and fibers: a practical alternative to tellurite for nonlinear fiber applications

H. Tilanka Munasinghe,[1] Anja Winterstein-Beckmann,[2] Christian Schiele,[3] Danilo Manzani,[1,4] Lothar Wondraczek,[2] Shahraam Afshar V.,[1] Tanya M. Monro,[1] and Heike Ebendorff-Heidepriem[1]

[(1)] *Institute for Photonics and Advanced Sensing, University of Adelaide, Adelaide, Australia*
[(2)] *Otto-Schott-Institute, University of Jena, Jena, Germany*
[(3)] *Department of Materials Science, University of Erlangen, Erlangen, Germany*
[(4)] *Institute of Chemistry, São Paulo State University, UNESP, CP 355, Araraquara, SP, 14801-970, Brazil*

tilanka.munasinghe@adelaide.edu.au

Abstract: We report on the fabrication of novel lead-germanate glasses and fibers. We have characterized these glasses in terms of their thermal properties, Raman spectra and refractive indices (both linear and nonlinear) and present them as viable alternatives to tellurite glasses for applications requiring highly nonlinear optical fibers.

OCIS codes: (060.2290) Fiber materials; (160.2750) Glass and other amorphous materials; (190.4400) Nonlinear optics, materials.

References and links

1. D. W. Hall, M. A. Newhouse, N. F. Borrelli, W. H. Dumbaugh, and D. L. Weidman, "Nonlinear optical susceptibilities of high-index glasses," App. Phys. Lett. **54**(14), 1293–1295 (1989).
2. H. Ebendorff-Heidepriem and T. M. Monro, "Extrusion of complex preforms for microstructured optical fibers," Opt. Express **15**(23), 15086–15092 (2007).
3. T. M. Monro and H. Ebendorff-Heidepriem, "Progress in microstructured optical fibres," Ann. Rev. Mater. Res. **36**(1), 467–495 (2006).
4. T. M. Monro, S. Warren-Smith, E. P. Schartner, A. François, S. Heng, H. Ebendorff-Heidepriem, and S. Afshar, "Sensing with suspended-core optical fibers," Opt. Fiber Technol. **16**(6), 343–356 (2010).
5. M. A. Ettabib, L. Jones, J. Kakande, R. Slavík, F. Parmigiani, X. Feng, F. Poletti, G. M. Ponzo, J. Shi, M. N. Petrovich, W. H. Loh, P. Petropoulos, and D. J. Richardson, "Phase sensitive amplification in a highly nonlinear lead-silicate fiber," Opt. Express **20**(2), 1629–1634 (2012).
6. N. Granzow, S. P. Stark, M. A. Schmidt, A. S. Tverjanovich, L. Wondraczek, and P. S. Russell, "Supercontinuum generation in chalcogenide-silica step-index fibers," Opt. Express **19**(21), 21003–21010 (2011).
7. N. Granzow, M. A. Schmidt, W. Chang, L. Wang, Q. Coulombier, J. Troles, P. Toupin, I. Hartl, K. F. Lee, M. E. Fermann, L. Wondraczek, and P. S. Russell, "Mid-infrared supercontinuum generation in As_2S_3-silica nano-spike step-index waveguide," Opt. Express **21**(9), 10969–10977 (2013).
8. S. Shahi, S. Harun, and H. Ahmad, "Multi-wavelength Brillouin fiber laser using a holey fiber and a bismuth-oxide based erbium-doped fiber," Laser Phys. Lett. **6**(6), 454–457 (2009).
9. D. G. Lancaster, S. Gross, H. Ebendorff-Heidepriem, K. Kuan, T. M. Monro, M. Ams, A. Fuerbach, and M. J. Withford, "Fifty percent internal slope efficiency femtosecond direct-written Tmˆ3+:ZBLAN waveguide laser," Opt. Lett. **36**(9), 1587–1589 (2011).
10. B. Richards, Y. Tsang, D. Binks, J. Lousteau, and A. Jha, "Efficient ˜2 μm Tmˆ3+-doped tellurite fiber laser," Opt. Lett. **33**(4), 402–404 (2008).
11. B. Richards, A. Jha, Y. Tsang, D. Binks, J. Lousteau, F. Fusari, A. Lagatsky, C. Brown, and W. Sibbett, "Tellurite glass lasers operating close to 2 μm," Laser Phys. Lett. **7**(3), 177–193 (2010).
12. A. Mori, Y. Ohishi, and S. Sudo, "Erbium-doped tellurite glass fibre laser and amplifier," Electron. Lett. **33**(10), 863–864 (1997).

#192254 - $15.00 USD Received 17 Jun 2013; revised 18 Aug 2013; accepted 18 Aug 2013; published 27 Aug 2013

13. A. Mori, H. Masuda, K. Shikano, and M. Shimizu, "Ultra-wide-band tellurite-based fiber aman amplifier," J. Lightwave Technol. **21**(5), 1300–1306 (2003).
14. P. Domachuk, N. A. Wolchover, M. Cronin-Golomb, A. Wang, A. K. George, C. M. B. Cordeiro, J. C. Knight, and F. G. Omenetto, "Over 4000 nm bandwidth of mid-IR supercontinuum generation in sub-centimeter segments of highly nonlinear tellurite PCFs," Opt. Express **16**(10), 7161–7168 (2008).
15. M. Liao, C. Chaudhari, G. Qin, X. Yan, T. Suzuki, and Y. Ohishi, "Tellurite microstructure fibers with small hexagonal core for supercontinuum generation," Opt. Express **17**(14), 12174–12182 (2009).
16. M. Liao, W. Gao, Z. Duan, X. Yan, T. Suzuki, and Y. Ohishi, "Directly draw highly nonlinear tellurite microstructured fiber with diameter varying sharply in a short fiber length," Opt. Express **20**(2), 1141–1150 (2012).
17. D. Buccoliero, H. Steffensen, H. Ebendorff-Heidepriem, T. M. Monro, and O. Bang, "Midinfrared optical rogue waves in soft glass photonic crystal fiber," Opt. Express **19**(19), 17973–17978 (2011).
18. H. Ebendorff-Heidepriem, C. Schiele, A. Winterstein, L. Wondraczek, D. G. Lancaster, D. J. Ottaway, and T. M. Monro, "New germanate glasses for infrared fibre applications," in *Proceedings of the 37th Australian Conference on Opt. Fibre Technol.*, paper no. 518.00 (Sydney, Australia, Dec 2013).
19. X. Jiang, J. Lousteau, and A. Jha, "The Structural, Thermal, and Opt. Analyses of Multicomponent Germanium Oxide Glasses for Engineering Mid-Infrared Fiber Chemical Sensing," J. Am. Ceram. Society **93**(10), 3259–3266 (2010).
20. J. Wu, Z. Yao, J. Zong, and S. Jiang, "Highly efficient high-power thulium-doped germanate glass fiber laser," Opt. Lett. **32**(6), 638–640 (2007).
21. X. Jiang, J. Lousteau, S. Shen, and A. Jha, "Fluorogermanate glass with reduced content of OH-groups for infrared fiber optics," J. Non-Cryst. Solids **355**(37-42), 2015–2019 (2009).
22. A. Lin, A. Ryasnyanskiy, and J. Toulouse, "Fabrication and characterization of a water-free mid-infrared fluorotellurite glass." Opt. Lett. **36**(5), 740–742 (2011).
23. M. F. Churbanov, A. N. Moiseev, A. V. Chilyasov, V. V. Dorofeev, I. A. Kraev, M. M. Lipatova, T. V. Kotereva, E. M. Dianov, V. G. Plotnichenko, and E. B. Kryukova, "Production of high-purity TeO2-ZnO and TeO2-WO3 glasses with the reduced content of OH-groups," J. Optoelectron. Adv. M. **9**(10), 3229–3234 (2007).
24. H. Ebendorff-Heidepriem, K. Kuan, M. R. Oermann, K. Knight, and T. M. Monro, "Extruded tellurite glass and fibers with low OH content for mid-infrared applications," Opt. Mater. Express **2**(4), 432–442 (2012).
25. X. Jiang, J. Lousteau, B. Richards, and A. Jha, "Investigation on germanium oxide-based glasses for infrared optical fibre development," Opt. Mater. **31**(11), 1701–1706 (2009).
26. A. Winterstein, S. Manning, H. Ebendorff-Heidepriem, and L. Wondraczek, "Luminescence from bismuth-germanate glasses and its manipulation through oxidants," Opt. Mater. Express **2**(10), 1320–1328 (2012).
27. M. R. Oermann, H. Ebendorff-Heidepriem, Y. Li, T.-C. Foo, and T. M. Monro, "Index matching between passive and active tellurite glasses for use in microstructured fiber lasers: Erbium doped lanthanum-tellurite glass," Opt. Express **17**(18), 15578–15584 (2009).
28. S. Manning, "Personal communication," Defence Science and Technol. Organisation (DSTO), Salisbury, Australia .
29. W. Q. Zhang, H. Ebendorff-Heidepriem, T. M. Monro, and S. Afshar V., "Fabrication and supercontinuum generation in dispersion flattened bismuth microstructured optical fiber," Opt. Express **19**(22), 21135–21144 (2011).
30. H. Ebendorff-Heidepriem, S. C. Warren-Smith, and T. M. Monro, "Suspended nanowires: fabrication, design and characterization of fibers with nanoscale cores," Opt. Express **17**(4), 2646–2657 (2009).
31. J. Bei, T. M. Monro, A. Hemming, and H. Ebendorff-Heidepriem, "Fabrication of extruded fluoroindate optical fibers," Opt. Mater. Express **3**(3), 318–328 (2013).
32. W. Vogel, *Glass chemistry* (Springer-Verlag, 1994).
33. J. S. Wang, E. Vogel, and E. Snitzer, "Tellurite glass: a new candidate for fiber devices," Opt. Mater. **3**(3), 187–203 (1994).
34. S. Manning, H. Ebendorff-Heidepriem, and T. M. Monro, "Ternary tellurite glasses for the fabrication of nonlinear optical fibres," Opt. Mater. Express **2**(2), 140–152 (2012).
35. J. Wang, J. R. Lincoln, W. S. Brocklesby, R. S. Deol, C. J. Mackechnie, A. Pearson, A. C. Tropper, D. C. Hanna, and D. N. Payne, "Fabrication and optical properties of lead-germanate glasses and a new class of optical fibers doped with Tm3+," J. App. Phys. **73**(12), 8066–8075 (1993).
36. V. Sigaev, I. Gregora, P. Pernice, B. Champagnon, E. Smelyanskaya, A. Aronne, and P. Sarkisov, "Structure of lead germanate glasses by Raman spectroscopy," J. Non-Cryst. Solids **279**(2-3), 136–144 (2001).
37. M. Dussauze, A. Giannoudakos, L. Velli, C. P. E. Varsamis, M. Kompitsas, and E. I. Kamitsos, "Structure and optical properties of amorphous lead-germanate films developed by pulsed-laser deposition." J. Chem. Phys. **127**(3), 34704 (2007).
38. V. Dimitrov and T. Komatsu, "An interpretation of optical properties of oxides and oxide glasses in terms of the electronic ion polarizability and average single bond strength," J. Univ. Chem. Technol. Metall **45**(3), 219–250 (2010).

#192254 - $15.00 USD Received 17 Jun 2013; revised 18 Aug 2013; accepted 18 Aug 2013; published 27 Aug 2013

39. M.D. O'Donnell, C.A. Miller, D. Furniss, V.K. Tikhomirov, and A.B. Seddon, "Fluorotellurite glasses with improved mid-infrared transmission," J. Non-Cryst. Solids **331**(1-3), 48–57 (2003).
40. Y. Abe and D. E. Clark, "Determination of combined water in glasses by infrared spectroscopy," J. Mater. Sci. Lett. **9**(2), 244–245 (1990).
41. C. A. Fenstermaker and F. L. McCrackin, "Errors arising from surface roughness in ellipsometric measurement of the refractive index of a surface," Surf. Sci., 85–96 (1969).
42. B. Johs and C. M. Herzinger, "Quantifying the accuracy of ellipsometer systems," physica status solidi (c) **5**(5), 1031–1035 (2008).
43. G. Jellison, "Data analysis for spectroscopic ellipsometry," Thin Solid Films **234**(1-2), 416–422 (1993).
44. H. Tompkins and E. A. Irene, *Handbook of Ellipsometry(Google eBook)* (William Andrew, 2005).
45. A. Boskovic, S. V. Chernikov, J. R. Taylor, L. Gruner-Nielsen, and O. A. Levring, "Direct continuous-wave measurement of n_2 in various types of telecommunication fiber at 155 m," Opt. Lett. **21**(24), 1966–1968 (1996).
46. G. Agrawal, *Nonlinear Fiber Optics (Google eBook)* (Academic Press, 2012).
47. S. Friberg and P. Smith, "Nonlinear optical glasses for ultrafast optical switches," IEEE J. Quantum Elect. **23**(12), 2089–2094 (1987).
48. P. Petropoulos, H. Ebendorff-Heidepriem, V. Finazzi, R.C. Moore, K. Frampton, D.J. Richardson, and T.M. Monro, "Highly nonlinear and anomalously dispersive lead silicate glass holey fibers," Opt. Express **11**(26), 3568–3573 (2003).
49. J. Bei, T. M. Monro, A. Hemming, and H. Ebendorff-Heidepriem, "Reduction of scattering loss in fluoroindate glass fibers," Opt. Mater. Express **3**(9), 1285–1301 (2013).

1. Introduction

The unique properties of soft glasses have seen them emerge recently as attractive materials for many optics applications. Foremost among these properties are: the high linear and nonlinear index [1]; relatively low melting temperatures (that enable them to be fabricated into complex structures via extrusion [2]); and broad transmission from the visible into the infrared [3]. Indeed soft glass optical materials have been used in sensing [4], optical signal processing [5], supercontinuum generation [6, 7] and laser applications [8, 9].

Amongst such materials, heavy metal oxide based glasses such as tellurite, germanate and gallate are popular choices for applications in the telecoms and mid IR bands (up to around 5 μm) where a high refractive index is required. In recent years, tellurite glasses in particular have demonstrated growing interest for mid-infrared fiber applications. These glasses have been used to fabricate both step-index and microstructured fibres. Step-index tellurite fiber has been used to demonstrate lasing at 2 μm [10,11] and fiber amplifiers [12,13], while the major interest in microstructured tellurite fibers to date has been for supercontinuum generation [14–16]. Recently, pumping at ~2 μm and extending the supercontinuum into the mid-infrared has been of growing interest [17].

Germanate glasses have similar phonon energies with correspondingly similar mid IR transmission properties. However, germanates have a higher glass transition temperature making them more mechanically and thermally stable than tellurite glasses [18, 19]. Thus they offer many of the same advantages whilst doing away with some of the main drawbacks found in the practical use of tellurite glass, making them attractive alternative materials for fiber applications in the mid-infrared [19]. Tm-doped step index germanate fibers, for example, have already been used to demonstrate high power lasing at ~2 μm [20]

When dealing with oxide glasses such as tellurite and germanate one must be mindful of the fact that they typically exhibit a high content of hydroxyl (OH) groups when melted in an ambient atmosphere. These OH groups are undesirable as they lead to intense and broad absorption at 3-4 μm. Several methods have been investigated to fabricate both tellurite and germanate glasses with low OH content, such as the use fluorides in the glass batch. However, this significantly changes the glass properties, making them more similar to those of fluoride glasses. This is undesirable for high gain lasers and nonlinear devices as it reduces the glass transition temperature and refractive index [21, 22]. To mitigate the effect of these OH groups we used a different approach, outlined in [23, 24] – where, for tellurite glasses, significant

#192254 - $15.00 USD Received 17 Jun 2013; revised 18 Aug 2013; accepted 18 Aug 2013; published 27 Aug 2013

reduction of the OH content (by 1-2 order(s) of magnitude) was achieved by using a controlled dry atmosphere for glass melting.

In this paper we report the fabrication and characterization of novel lead-germanate glasses, and evaluate the use of these glasses for nonlinear applications where, to date, tellurite glasses with comparatively low mechanical and thermal stability have been extensively investigated. Lead-germanates are of particular interest since, within the germanate family, they show the highest refractive index and their suitability for step-index fiber fabrication has previously been demonstrated [19, 25]. They have also been shown to be highly transparent in the visible spectral range [25], unlike bismuth germanates which exhibit complex absorption phenomena (associated with the bismuth species) that span the visible to near IR range [26]. For a Na-Zn-tellurite glass, addition of La_2O_3 increased the glass stability and allowed incorporation of active rare earth ions without significantly changing the glass properties [27]. Building on these results, we investigated in this paper, the impact of La_2O_3 on the glass stability, and thermal and optical properties of lead-germanate glass. In addition to this, the linear index for some glass compositions was measured, via the ellipsometry technique, over the range from approximately 500 nm to 2 μm.

Where appropriate, the analyzed properties of our lead-germanate glasses have been compared with a Zn-tellurite glass. We chose to compare with Zn-tellurite since these glasses have been widely investigated for mid-IR applications [10, 12, 14–16] and such a comparison would enable us to study the suitability of our germanate glasses as a practical alternative to tellurite. Within the Zn-tellurite glass system, we have selected a Na-Zn-La tellurite glass (TZNL) whose properties we investigated in detail and which has been optimized for fabrication of microstructured fibers using the extrusion technique [27], and the same technique was used to fabricate the lead-germanate microstructured fiber in this paper.

To evaluate whether our germanate glasses lend themselves to high nonlinearity fiber fabrication, we also report on the first germanate microstructured fiber – manufactured using the extrusion technique to generate the preform from which the fiber was drawn. Using this fiber we were also able to characterize the nonlinear refractive index of one of the compositions at 1550 nm via a measurement of the effective fiber nonlinearity.

2. Glass and fiber fabrication

2.1. Glass samples for thermal and optical characterization

We prepared two series of glasses within the system $60{\cdot}GeO_2$ — $(40-x-y){\cdot}PbO$ — $x{\cdot}La_2O_3$ — $y{\cdot}Na_2O$ (Table 1) with x ranging from 0 to 10 and $y = 0$ or 5 (Table 1). The glasses were prepared using 30-300 g batch weights. The commercially available raw materials (American Elements, Alfa Aesar, Sigma-Aldrich) used were GeO_2, PbO, La_2O_3 and Na_2CO_3 with 99.99% or higher purity. The glass batches were prepared in a glovebox purged with dry nitrogen ($\leq$10 ppmv water). All glasses were melted in platinum crucibles at 1250 °C for 0.5-5 h, depending on the batch weight. The glass melts were cast into preheated brass moulds and annealed at 400-450 °C, depending on the glass composition and batch weight. The majority of the glasses used for thermal and spectroscopic measurements and unstructured fiber fabrication were melted, swirled, cast and annealed in ambient atmosphere. A few glasses were melted, swirled, cast and annealed in dry atmosphere using a melting facility comprising a melting furnace purged with a gas mixture with similar composition to air (80% nitrogen and 20% oxygen), an annealing furnace and glovebox purged with dry nitrogen. The water content of the gases used was 10 ppmv.

We fabricated three different types of glass samples: rectangular glass blocks of dimensions $15\times10\times30$ mm^3 for thermal and spectroscopic measurements, cylindrical glass billets of 30 mm diameter and ~30 mm height for unstructured fiber fabrication, and cylindrical glass

#192254 - $15.00 USD Received 17 Jun 2013; revised 18 Aug 2013; accepted 18 Aug 2013; published 27 Aug 2013

billets of 50 mm diameter and ~20 mm height for suspended core fiber fabrication.

Polished plates made from the glass blocks or polished billets were used to measure the IR absorption and the linear refractive index. The glass blocks as a whole were used for density measurements, and glass pieces from blocks were used for thermal analysis measurements.

The properties of the fabricated germanate glasses were compared with that of a Na-Zn-tellurite glass (TZNL) with nominal composition (in mol%) of $73{\cdot}TeO_2$ — $20{\cdot}ZnO$ — $5{\cdot}Na_2O$ — $2{\cdot}La_2O_3$. The fabrication of glass and fiber samples of this tellurite glass composition is described in [24, 27].

Table 1. Nominal glass composition (in mol%), density, glass transition temperature (T_g), onset of glass crystallization (T_x), glass stability ($T_x - T_g$), linear (n_0) and nonlinear (n_2) indices of germanate glasses made and tellurite glass TZNL published in [27][f].

Glass code	GeO_2	PbO	La_2O_3	Na_2O	Density (g/cm^3)	T_g (°C)	T_x (°C)	T_x-T_g (°C)	n_0 at 1.55 µm	n_2 (10^{-20} m^2/W)
GP	60	40			6.27	422	570	148		
GPL2	60	38	2		6.24	444	576	132		
GPL5	60	35	5		6.16	478	598	120	1.916	
GPL10	60	30	10		6.13	cast glass partially crystallized				
GPN	60	35		5	5.90	395	608	213		
GPNL2	60	33	(2)[a]	5	5.93	415	663	248	1.869	
GPNL5	60	30	5	5	5.83	455	692	244	1.868	57
TZNL	(73)[b]	(20)[c]	2	5	5.37[d]	315[d]	480[d]	165[d]	1.983[d]	55[e]

[a] For this sample, 2mol% Tm_2O_3 instead of La_2O_3 was used.
[b] This value refers to the TeO_2 content.
[c] This value refers to the ZnO content.
[d] Values taken from [27].
[e] Value taken from [28].
[f] The measurement errors for the germanate glass properties are ±0.01 g/cm^3 for the density, ±2 °C for T_g and T_x, ± 0.02 for n_0 and ± 6.3×10^{-20} m^2W^{-1} for n_2.

2.2. Fiber fabrication for loss, Raman and nonlinear index measurements

We fabricated unstructured fibers using GPL5 and GPNL5 glass and a suspended core fiber [4] using GPNL5 glass. We used the extrusion technique to produce both unstructured preforms (10mm diameter rods) and the suspended core preform. While unstructured preforms can be made directly by casting, we used the extrusion technique for the following reason. The extrusion technique is a versatile method for the production of low-loss microstructured optical fibers with various shapes produced from different types of glasses [2, 29, 30] including suspended small-core fibers that are particularly suited for nonlinear processing applications. Therefore, we used the extrusion technique to demonstrate suspended core fiber fabrication for GPNL5 glass composition, which offers both high glass transition temperature and high glass stability (see Section 3.1). In order to evaluate the suitability of the extrusion technique for our germanate glasses, we also produced the unstructured preforms via extrusion. In addition, it has been demonstrated that the extrusion method is suitable for the preparation of bubble-free rods which typically exhibit better surface finish and fewer bubbles than cast rods [31].

To fabricate the fibers, we first extruded 30-50 mm diameter glass billets into preforms using the billet extrusion technique [2]. The billets were extruded in ambient atmosphere through stainless steel dies at 510-530 °C with a volume flow rate of 2.4 mm^3/s. For unstructured fiber fabrication, billets made in ambient atmosphere were extruded to rods (10 mm diameter). For

#192254 - $15.00 USD Received 17 Jun 2013; revised 18 Aug 2013; accepted 18 Aug 2013; published 27 Aug 2013

suspended core fiber fabrication, a billet made in dry atmosphere was extruded to a suspended core preform (15 mm outer diameter, 1 mm core diameter) (Fig. 1(a)), and a billet made in ambient atmosphere was extruded to a tube (10 mm outer diameter, 1 mm inner diameter). All extruded items were annealed at 420-440 °C in ambient atmosphere.

The cane and fibers were drawn from the extruded preforms using a fiber drawing tower. The tower furnace body was purged with a mixture of 70% nitrogen and 30% oxygen, which had the same purity as the gases used for glass melting. The extruded rods of GPL5 and GPNL5 composition (Table 1) were directly drawn down to unstructured (unclad) fibers of 160 μm outer diameter. The suspended core fiber was made from GPNL5 glass preform in two steps. First the suspended core preform was scaled down to a cane of 1 mm outer diameter. Then the cane was inserted into the tube, and this assembly was drawn down to a fiber of 160 μm outer diameter. Using scanning electron microscopy (SEM) cross-sectional image of the suspended core fiber (Fig. 1(b)), the core diameter (i.e. the diameter of the largest circle that can be inscribed in the triangular core region) was measured to be 1.55 μm.

The unstructured fibers were used for fiber loss and Raman measurements, whereas the suspended core fiber was used for nonlinear index and loss measurements.

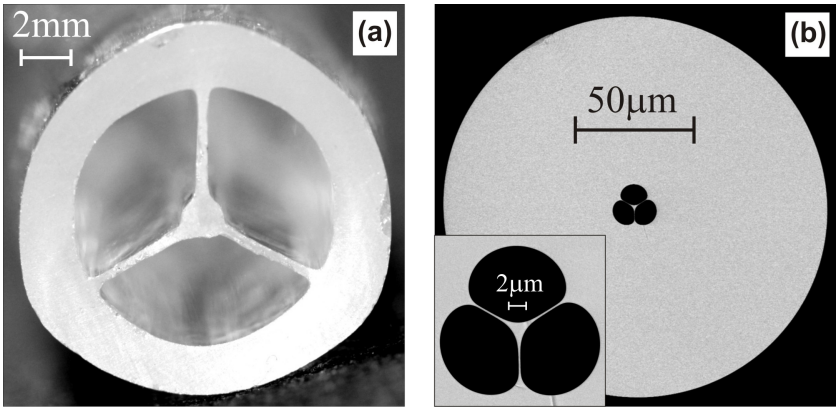

Fig. 1. (a) Photograph of suspended core lead germanate preform, and (b) SEM image of the first lead germanate suspended core fiber.

3. Glass properties

3.1. Density and thermal analysis

The density of the glasses was measured using the buoyancy method. Not surprisingly, the density of the Na-free germanate glasses (6.1-6.3 g/cm^3) is significantly higher than that of the Na-containing glasses (5.8-5.9 g/cm^3). Both types of germanate glasses have a higher density compared with Na-Zn-tellurite glass (Table 1), which is attributed to the high amount of the heavy metal oxide PbO.

The glass transition temperature (T_g) and onset of glass crystallization temperature (T_x) were measured using differential scanning calorimetry (DCS) on 30-60 mg glass disks with a heating rate of 20 K/min. The temperature difference T_x-T_g is used as a measure of the glass stability.

Figure 2(a) shows the glass transition temperature as a function of increasing La_2O_3 content of the germanate glasses. For both the Na-free and the Na-containing glasses, the T_g increases with increasing replacement of PbO by La_2O_3, which is of benefit for developing glasses with higher thermal stability

Within the Na-free glasses, the glass stability ($T_x - T_g$) slightly decreases as PbO is

#192254 - $15.00 USD Received 17 Jun 2013; revised 18 Aug 2013; accepted 18 Aug 2013; published 27 Aug 2013

increasingly replaced with La_2O_3 (Fig. 2(a)). For the glass GPL10 with 10 mol% La_2O_3, crystals were observed in the glass melt before casting. This result indicates that larger amounts of La_2O_3 (> 5 mol%) in GPLx results in low glass stability and thus make the glass unsuitable for fiber fabrication.

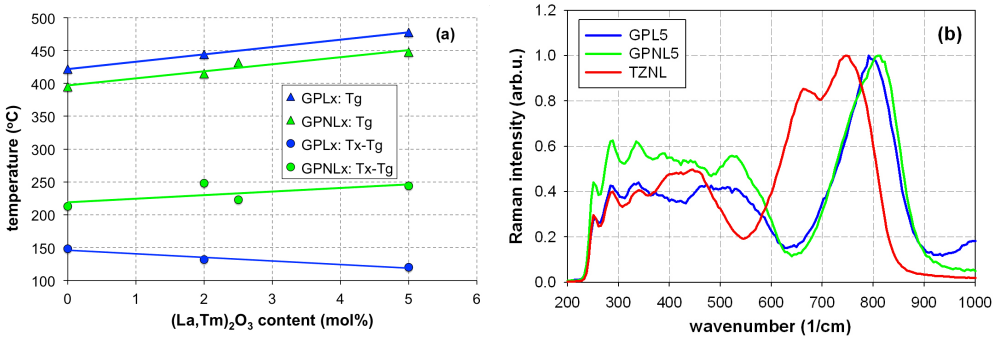

Fig. 2. (a) Glass transitin temperature (T_g) as a function of the $(La,Tm)_2O_3$ content of Na-free germanate glasses (GPL) and Na-containing germanate glasses (GPNL), and (b) Raman spectra of germanate glasses (GPL5, GPNL5) and tellurite glass (TZNL).

Compared with the Na-free germanate glasses, the Na-containing glasses have a considerably higher glass stability. This result is consistent with the glass stabilizing effect of small amounts of Na_2O in lead-silicate and tellurite glasses [32, 33]. Within the Na-containing glasses, the glasses with La_2O_3 have a slightly higher glass stability than the glass without La_2O_3, which demonstrates that the presence of Na_2O enhances the solubility of La_2O_3 in the glass matrix.

3.2. Raman spectra

The Raman spectra were measured for the two unstructured fibers made from GPL5 and GPNL5 glasses and for a TZNL unstructured fiber made also using the extrusion technique as described in [27]. An argon ion continuous wave laser beam at 514.5 nm was launched into a fiber piece of ~30 cm length. We used low power of 56 mW to avoid photo-induced structural changes. From the same fiber end, the output light was imaged onto a spectrometer (Horiba Jobin Yvon - iHR 320). The laser line was blocked using a bandpass filter. This filter caused the Raman spectra to be cut-off at 250 cm^{-1}. The wavelength of the spectrometer was calibrated using the argon ion laser line at 514.5 nm. Note that the same Raman spectrum was obtained using higher energy laser beam at 488 nm, indicating that photo-induced structural changes did not occur under our experimental conditions.

Figure 2(b) shows the Raman spectra for the two germanate fibers and the tellurite fiber. For both germanate glasses, the highest-frequency Raman band is situated at ~800 cm^{-1}. This Raman band is composed of two peaks attributed to Ge-O stretching vibrations [19]. The highest-frequency Raman band of the tellurite fiber is at 750 cm^{-1} and is composed of two peaks attributed to Te-O stretching vibrations [34] . The position of the highest-frequency Raman bands agrees with other tellurite and lead-germanate glasses [19, 34–37].

The frequency of diatomic molecule stretching vibrations increases with increasing bond strength and decreasing mass of the atoms [32]. Therefore, the shift of the network former stretching vibration to higher frequency from Te-O to Ge-O is attributed to both the higher bond strength of Ge-O (due to higher field strength of Ge^{4+} compared with Te^{4+} [38]) and lower mass of Ge compared with Te.

#192254 - $15.00 USD Received 17 Jun 2013; revised 18 Aug 2013; accepted 18 Aug 2013; published 27 Aug 2013

3.3. IR absorption spectra of bulk glass samples

To determine the position of the IR edge and the OH content of the glasses, we measured the absorption spectra in the mid-infrared at 2-6 μm. For these measurements, polished glass samples of 2-20 mm thickness were prepared from the glass blocks or billets. Transmission spectra in the wavelength range of 2-10 μm were measured using commercial FTIR spectrometer (PerkinElmer FTIR 400). Background absorbance due to Fresnel reflection and sample surface imperfection were subtracted from the measured spectra prior to calculation of the attenuation loss in dB/m (which is connected to the absorption coefficient α in cm^{-1} by $\text{loss} = 1{,}000 \cdot \alpha / \ln 10$). The measurement error is ±5 dB/m.

Figure 3(a) shows the IR spectra for several Na-free and Na-containing germanate glasses and also for TZNL tellurite glass melted in ambient atmosphere. All glasses showed a high OH content, shown by the high absorption intensity of the OH bands at 3.0-3.4 μm and 4.3-4.4 μm, due to melting in ambient atmosphere. As demonstrated in [24] for tellurite glass, the high water content of glasses melted in ambient atmosphere is not due to incorporation of water from the atmosphere into the melt but due to the water content of the raw materials. Figure 3 also illustrates that the IR edge of lead-germanate glasses is shifted by ~0.5 μm towards shorter wavelengths compared with the Na-Zn-tellurite glass. This result is consistent with the higher phonon energy of lead-germanate glass (~800 cm^{-1}) compared with Na-Zn-tellurite glass (750 cm^{-1}) as described in Section 3.2.

For multicomponent glasses, the broad OH band at 3.0-3.4 μm is composed of a narrow band at 3.0 μm due to free OH groups, and a broad band at 3.3 μm due to weakly hydrogen bonded OH groups. The band at 4.3-4.4 μm is attributed to strongly hydrogen bonded OH groups [39]. To investigate the impact of glass composition on these OH bands, we normalized the IR spectra to the maximum OH absorption at 3.0-3.4 μm (Fig. 3(b)). The germanate glasses and the tellurite glass exhibit significantly different shapes of the OH band combining free and weakly bonded OH groups. For the germanate glasses, this OH band has its peak at 3.0 μm and a shoulder at 3.5 μm, indicating that the free OH groups have higher peak intensity than the weakly bonded OH groups. In contrast, for the tellurite glass, the OH band peak is shifted to longer wavelength of 3.4 μm and a shoulder is observed at shorter wavelength of 3.0 μm, indicating that the free OH groups have a lower peak intensity than the weakly bonded OH groups. Assuming similar extinction coefficient for free and weakly bonded OH groups in germanate and tellurite glasses, the different intensities for the two types of OH groups demonstrates that the ratio of weakly bonded OH groups to free OH groups is larger in tellurite glasses compared with germanate glasses. As weakly bonded OH groups form hydrogen bonds to non-bridging oxygens (NBO) [40], the higher ratio of weakly bonded to free OH groups in tellurite glasses indicates that tellurite glasses have more NBOs compared with germanate glasses. This appears to be in contradiction to the lower amount of network modifier oxides in the tellurite glass (27%) compared with the germanate glasses (40%). Therefore, we suggest that the larger amount of hydrogen-bonded OH groups in tellurite glass is caused by the formation of hydrogen bonds to the lone electron pairs of TeO_3 and TeO_4 groups. The absence of lone electron pairs for GeO_4 groups leads to a higher number of free OH groups.

The OH band at ~3 μm has the same shape for all Na-free germanate glasses and also for all the Na-containing germanate glasses (Fig. 3(b)). This result indicates that replacement of PbO with La_2O_3 does not affect the position and intensity ratio of the free and weakly bonded OH groups.

The OH-band at ~3 μm has slightly different shape for Na-free and Na-containing germanate glasses. The higher intensity of the shoulder of the Na-containing glasses indicates higher ratio of weakly bonded OH to free OH compared with the Na-free germanate glasses. This result suggests that the replacement of PbO with Na_2O increases the amount of NBOs and thus the

#192254 - $15.00 USD Received 17 Jun 2013; revised 18 Aug 2013; accepted 18 Aug 2013; published 27 Aug 2013

amount of weakly bonded OH groups relative to free OH groups.

The band of the strongly bonded OH groups has similar width and intensity in all of the germanate and tellurite glasses investigated. The position of the band is shifted to slightly longer wavelength for the tellurite glass compared with the germanate glasses.

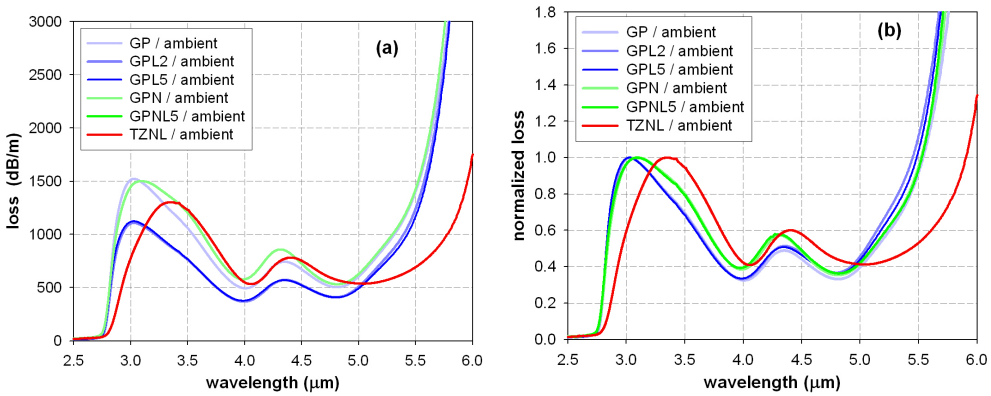

Fig. 3. IR absorption spectra of bulk glass samples melted in ambient atmosphere: (a) spectra in dB/m, and (b) spectra normalized to the OH peak at ~3 μm.

Figure 4(a) compares the IR spectra of GPL5, GPNL5 and TZNL glass samples melted in ambient and dry atmosphere. For all three glasses, use of dry atmosphere led to a decrease of the absorption intensity of the main OH band by a factor of 6-9 for the germanate glasses and a factor of 13 for the tellurite glass. For tellurite glasses, it was shown that the decrease in OH content when melting in dry atmosphere is in particular dependent on the melting time and glass melt volume [24]. Note that the results of the germanate glasses shown here are of preliminary melting trials in dry atmosphere without optimization of the melting time for a melt volume. Systematic melting trials in dry atmosphere are expected to lead to further reduction in the OH absorption of the germanate glasses.

Normalization of the IR spectra of the glasses melted in ambient and dry atmosphere to the maximum OH absorption at 3.0-3.4 μm (Fig. 4(b)) reveals that for the Na-containing glasses GPNL5 and TZNL the shape of the OH band comprising free and weakly bonded OH groups remains identical when reducing the OH content via melting in dry atmosphere. For the Na-free germanate glass GPL5, the ~3 μm OH band of the glass melted in dry atmosphere is slightly shifted to longer wavelengths and the shape resembles that of the GPNL5 glass. This result indicates that dehydration of the GPL5 glass melt led to a slight increase in the number of weakly bonded OH relative to free OH groups. In other words, melting of GPL5 in dry atmosphere preferentially decreased the amount of free OH groups relative to hydrogen-bonded OH groups. However, further investigations are required to substantiate this conclusion.

The normalization of the spectra (Fig. 4(b)) also shows that dehydration does not lead to an equal reduction in absorption intensity in the region of the two OH bands, i.e. in the regions 2.7-4.0 μm and 4.0-5.0 μm. We attribute this behavior to the following: the absorption in the region 4.0-5.5 μm is a superposition of the OH band at ~4.4 μm and an intrinsic absorption being a tail of the steep IR edge at $>$ 5.5 μm for germanate glasses and $>$ 5.9 μm for the tellurite glass. In the case of complete removal of OH groups, the absorption of this IR edge tail would limit the IR transmission of fibers with $>$ 1 m length (i.e. for fiber losses $<$ 1dB/m) to ~4 μm for both germanate and tellurite glasses. Overall, we see that by melting in a dry atmosphere we are able to achieve similar reductions in OH band losses for both germanate

#192254 - $15.00 USD Received 17 Jun 2013; revised 18 Aug 2013; accepted 18 Aug 2013; published 27 Aug 2013

and TZNL glasses.

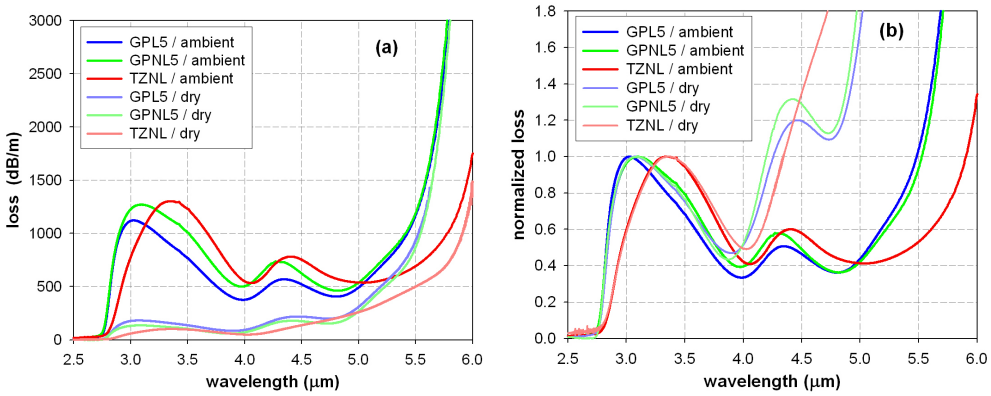

Fig. 4. IR absorption spectra of bulk glass samples melted in ambient and dry atmosphere: (a) spectra in dB/m, and (b) spectra normalized to the OH peak at ~3μm.

3.4. Visible-IR loss of unstructured fibers

To determine the material loss that can be achieved in extruded germanate glass fibers, we measured broadband fiber loss spectra for the GPL5 and GPNL5 unstructured fibers using the standard cutback technique. The light source was a tungsten filament bulb, and the fiber output was coupled via a bare fiber adaptor to a commercial optical spectrum analyzer ranging from 400-1700 nm. We performed several cleaves for each cutback length to ensure that cleave variability did not impact the results. The measurement error is 10%.

Figure 5(a) shows the loss spectra of GPL5, GPNL5 and TZNL unstructured fibers. All three fibers have a similar minimum loss of 0.5-1 dB/m at ~1.3 μm. Preliminary absolute absorption measurements of the bulk GPNL5 glass indicated that reduction of the minimum loss of germanate glass fibers to ~0.2 dB/m is possible by improving the extrusion and fiber drawing conditions.

The band at 1.45 μm is the overtone of the fundamental absorption of free OH groups at ~3.0 μm [24]. The higher intensity of the overtone of free OH groups in germanate glasses compared with tellurite glass is consistent with the larger intensity the fundamental absorption of free OH groups in germanate glasses (Section 3.3 and Fig. 4(a)).

The shift of the free OH overtone from 1.44 μm in the germanate glasses to 1.47 μm in the tellurite glass is consistent with the wavelength shift of the fundamental vibration of strongly bonded OH groups (4.3 μm for germanate and 4.4 μm for tellurite). Due to the overlap of the fundamental vibrations of free and weakly bonded OH groups, any wavelength shift cannot be resolved for these two vibration bands. We attribute the red shift of the OH bands, i.e. the shift to lower frequency, from germanate to tellurite glasses to decreasing bond strength from Ge-O to Te-O similarly to the lower frequency shift from the Ge-O to the Te-O stretching vibration observed in the Raman spectra (Section 3.2 and Fig. 2(b)).

For tellurite glass, we found that melting in a platinum crucible (compared with melting in a gold crucible) results in additional absorption at $\leq$ 600 nm due to the presence of platinum impurities in the glass as a result of crucible corrosion by the glass melt [24] (Fig. 5(a)). The short wavelength edge of our germanate fibers is at a similar position as that of the tellurite glass fiber made from glass melted in a platinum crucible. This result indicates that in germanate glass fibers the short wavelength loss is limited by the absorption of platinum species and not by the

#192254 - $15.00 USD Received 17 Jun 2013; revised 18 Aug 2013; accepted 18 Aug 2013; published 27 Aug 2013

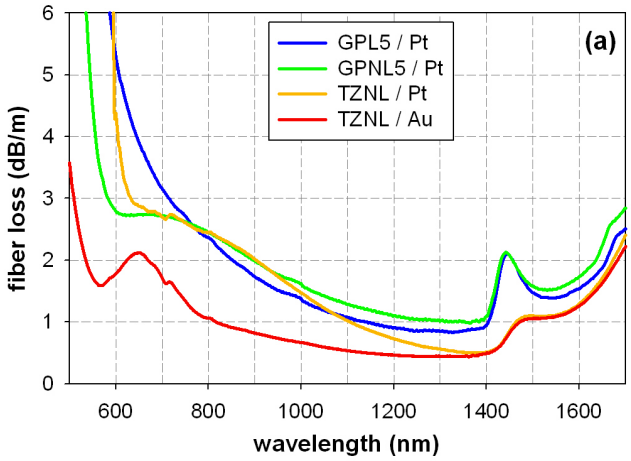

Fig. 5. (a) Loss spectra of unstructured fibers. (b) Refractive indices of of GPL5, GPNL2 and GPNL5 germanate glasses and TZN tellurite glass. Circles are measured points; the line shows the Sellmeier fit.

intrinsic absorption edge of the glass.

3.5. Linear refractive index and material dispersion

For the GPL5, GPNL2 and GPNL5 germanate glasses and for a TZN tellurite glass (in mol%: 80·TeO_2 — 10·ZnO — 10·Na_2O) with similar composition to TZNL, the linear refractive index was measured over the broad range of 500-2000 nm using spectroscopic ellipsometry – a broad band technique that measures the change in polarization of light as it reflects from (or transmits through) a material. The measured response depends on the dielectric properties and thickness of the material and can therefore be used to infer the values of optical constants, such as the refractive index.

For this investigation we used an ellipsometer provided by the J. A. Woollam company in fairly typical ellipsometry configuration: linearly polarized light was reflected from the sample surface and the reflected beam analyzed via a rotating polarizer to determine the ellipticity of its polarization. By comparing the polarization ellipse of the reflected light with the known linear polarization of the incident light, the system is able to determine the change in both amplitude and phase of the *s*-polarized and *p*-polarized constituents. This change in polarization is represented by the complex reflectance ratio ρ, given below in terms of parameters Ψ and Δ

$$\rho = \tan(\Psi)e^{i\Delta} = \frac{\widetilde{R}_s}{\widetilde{R}_p} \tag{1}$$

where $\widetilde{R}_s$ and $\widetilde{R}_p$ are the Fresnel reflection coefficients of the *s*-polarized and *p*-polarized light, respectively.

Since ellipsometry measures a change in polarization, anything that contributes to depolarization, such as surface roughness, will add error to the results. To minimize such errors glass samples of 8-10 mm thickness were prepared with a finely polished surface to ensure that the average surface roughness, R_a, was as low as possible. Analysis of the effect of surface roughness on the apparent value of the refractive index in [41] shows that for glass samples, a negligible effect is observed for roughness values up to 30 nm. We measured the R_a of our

#192254 - $15.00 USD Received 17 Jun 2013; revised 18 Aug 2013; accepted 18 Aug 2013; published 27 Aug 2013

samples with a surface profiler to be approximately 15 nm to 20 nm for all the samples, which is well under this threshold.

In addition to carefully polishing the surface we also averaged over each spectral point (100 scans per point) and incidence angle (12 scans per angle, 5 angles). Given the bulk nature of our samples (i.e. not thin films), the surface polishing and the high averaging, we estimate that the error in our measurements is no more than 1-2% [42–44].

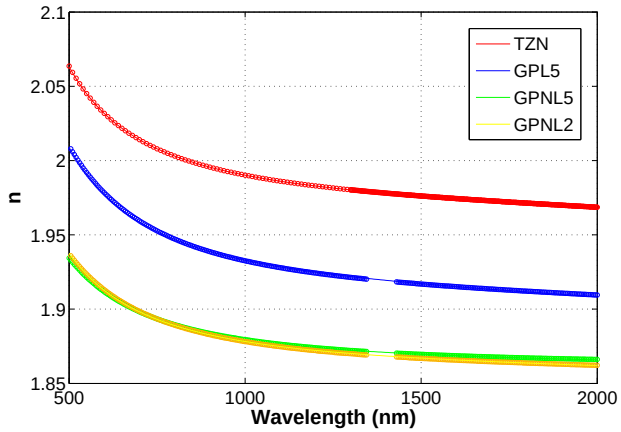

Fig. 6. Refractive indices of of GPL5, GPNL2 and GPNL5 germanate glasses and TZNL tellurite glass. Circles are measured points; the line shows the Sellmeier fit.

The results of the refractive index measurement, in the visible and near IR range, are shown in Fig. 6. From these measurements we are able to fit a Sellmeier equation of the form shown in Eq. (2) to the data.

$$n^2(\lambda) = 1 + \sum_{i=1}^{3} \frac{B_i \lambda^2}{\lambda^2 - C_i} \tag{2}$$

The values of the fitted Sellmeier coefficients are given in Table 2. The values at 1.55 μm are listed in Table 1.

Table 2. Sellmeier coefficients for germanate and tellurite glasses

Glass	B_1	B_2	B_3	C_1	C_2	C_3
GPL	1.458	1.203	23.06	0.03138	0.03064	2287.0
GPLN5	1.065	1.399	1.849	0.02663	0.02663	2555.6
GPLN2	1.538	0.934	1.120	0.01417	0.04078	782.1
TZN	1.378	1.511	3.435	0.04756	0.00744	411.3

Not surprisingly, the Na-free germanate glass GPL5 has a significantly higher index that the Na-containing glasses GPNL2 and GPNL5 (Fig. 6). This result is consistent with the higher density for Na-free germanate glasses as described in Section 3.1. Despite different content of the heavy metal oxide PbO and different density, GPNL2 and GPNL5 exhibit almost identical refractive indices. In GPNL2 and GPNL5, 2mol% and 5mol% PbO are replaced with Tm_2O_3 and La_2O_3, respectively. Both Tm_2O_3 and La_2O_3 are lanthanide oxides (Ln_2O_3). Hence, the almost identical refractive indices of GPNL2 and GPNL5 indicate that PbO and Ln_2O_3 have comparable impact on the refractive index.

#192254 - $15.00 USD Received 17 Jun 2013; revised 18 Aug 2013; accepted 18 Aug 2013; published 27 Aug 2013

The lead-germanate glasses have somewhat lower indices than the TZN and TZNL tellurite glasses, which is attributed to the lower polarizability of Ge^{4+} compared with Te^{4+} [38].

3.6. Nonlinearity measurement

The nonlinear refractive index for the GPNL5 suspended core fiber was determined by first calculating the value of the nonlinear coefficient (using the method described in [45]), which is based on measuring the phase shift, ϕ, induced by the Self Phase Modulation (SPM) phenomenon [46]. It involves pumping a fiber with a dual frequency signal and observing the generation of sidebands via Four Wave Mixing (FWM) [46]. The relative ratio of the spectral components is then used to determine ϕ as a function of the average signal power $\bar{P}$. This relationship is given below.

$$\phi = 2\gamma L_{eff}\bar{P} \tag{3}$$

In Eq. (3) above, γ is the nonlinear coefficient and L_{eff} is the effective length. γ is defined as below.

$$\gamma = \frac{2\pi}{\lambda}\frac{n_2}{A_{eff}} \tag{4}$$

where n_2 is the nonlinear refractive index, λ is the central wavelength, A_{eff} is the effective area of the fiber mode and L_{eff} is defined as below.

$$L_{eff} = (1 - e^{-\alpha L}) \tag{5}$$

where α and L represent the absorption coefficient and length of the fiber, respectively.

The experimental setup we used is shown in Fig. 7. The CW pump lasers were set to 1553.50 nm and 1553.87 nm before being coupled into an Erbium Doped Fiber Amplifier (EDFA). The EDFA was used to amplify power of each pump from approximately 3 mW up to approximately 800 mW (measured just before the fiber input). This light was then launched into the test fiber. In our experiment we used the suspended core fiber made from GPNL5 glass (see Section 2).

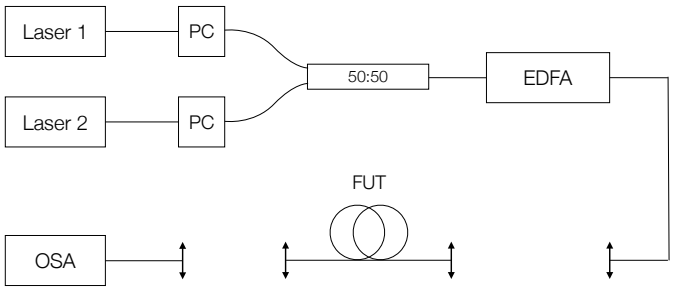

Fig. 7. Experimental setup. Light from the two lasers was coupled into a 50:50 coupler via a pair of Polarization Controllers (PCs) and then sent to an Erbium Doped Fiber Amplifier (EDFA). The pump light was then collimated and coupled into the Fiber Under Test (FUT) through appropriate lenses. The fiber output was then finally collected into an Optical Spectrum Analyzer (OSA)

#192254 - $15.00 USD Received 17 Jun 2013; revised 18 Aug 2013; accepted 18 Aug 2013; published 27 Aug 2013

After propagation through the fiber light was collected into a patch cable before being fed into an Optical Spectrum Analyzer (OSA). In order to improve accuracy multiple spectra were collected for each signal power, so that they could be averaged over. A set of these is shown in Fig. 8(a) for various signal powers. By taking the ratio of the pump peak power to the sideband peak power we were able to obtain a value for ϕ at each signal power (details of this calculation can be found in [45]). We then plot the nonlinear phase shift as a function of average signal power in order to extract the slope and thus γ. A plot of this phase shift is shown in Fig. 8(b).

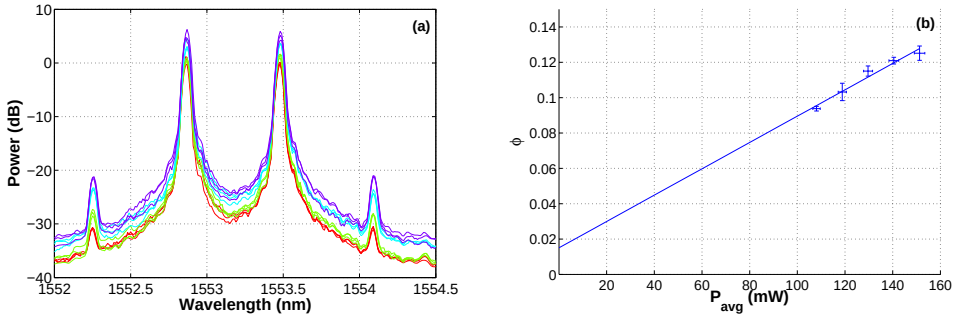

Fig. 8. (a) Four Wave Mixing (FWM) spectrum obtained at output of fiber showing pumps at 1553.50 nm and 1553.87 nm, and first order sidebands. (b) Phase shift measurement. For this fiber we measured the length to be 56.6 cm and the loss, α, to be 8.0 ± 0.8 dB/m.

The suspended core fiber used in the experiment was made from a larger billet (180 g) melted for the first time in a controlled atmosphere glass melting facility. Due to unoptimized conditions for this first large glass melt, particles from the furnace liner were unintentionally introduced into the melt. As a result, the fiber had sections of varying loss. In order to account for this in our measurements, we used fiber pieces with relatively short lengths and measured both the nonlinearity and the loss for these pieces. The loss of these fiber pieces varied from 4.5 to 8.8 dB/m. Given that this is a first generation fiber of this material and structure we are confident that, in future trials, the loss can be made consistent and lowered to a value much closer to the measured bare fiber loss for this material, i.e. < 1.5 dB/m at 1550 nm.

From the slope of the phase shift curve in Fig. 8(b) and the measured values for length and loss we are able to determine that $\gamma = 1177 \pm 128$ W^{-1}km^{-1} for this fiber. In order to calculate the effective area A_{eff} we took a SEM image of the fiber used in the experiment and inserted it into a finite element model (COMSOL Multiphysics) to find the electric and magnetic fields of the fundamental mode propagating through the fiber; A_{eff} was then calculated to be 1.951 μm^2 [46]. By then using the equation $\gamma = 2\pi n_2/\lambda A_{eff}$ we were able to extract a value for the nonlinear refractive index: $n_2 = 56 \pm 6 \times 10^{-20}$ m^{2}W^{-1}.

The nonlinear index of the TZNL glass was measured to be $n_2 = 55 \pm 2 \times 10^{-20}$ m^{2}W^{-1} [28] for a polished glass plate using the Z-scan technique as described in [34]. Within the measurement error, the nonlinear indices of TZNL and GPNL5 glass are identical.

In Fig. 9 we compare our measured value for the optical nonlinearity with values found in the literature for other soft glasses, including lead-germanates. For those other lead-germanates, the n_2 values have been obtained by converting the third order optical susceptibility $\chi^{(3)}$ values measured by Hall *et. al.* [1] using:

$$n_2 \text{ [m}^2\text{/W]} = K \frac{160\pi}{c n_0^2} \chi^{(3)} \text{ [esu]} \tag{6}$$

where n_0 is the linear index, c is the speed of light and K is a constant. Whilst there is some

#192254 - $15.00 USD Received 17 Jun 2013; revised 18 Aug 2013; accepted 18 Aug 2013; published 27 Aug 2013

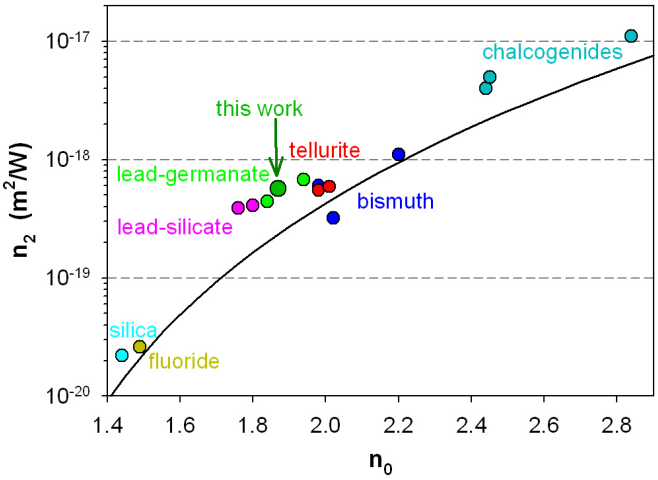

Fig. 9. Nonlinear index of GPNL5 compared with other soft glasses. Solid line is Miller curve as per [3].

uncertainty in the literature as to the appropriate value of this constant, we chose $K = 6$ as this value converts, for lead-silicate glass, the $\chi^{(3)}$ [esu] value measured by Hall to an n_2 [m^2/W] value that is similar to the n_2 value which was measured by Friberg *et. al.* [47] and independently confirmed by Petropoulos *et. al.* [48].

We note that the relationship between the linear and nonlinear index for our lead-germanate glass agrees well with those measured by Hall *et. al.* [1] for $60{\cdot}GeO_2$ — $40{\cdot}PbO$ and $75{\cdot}GeO_2$ — $25{\cdot}PbO$ glasses. To the best of our knowledge, these are the only other measurements of the optical nonlinearity of lead-germanate glasses to date.

4. Conclusion

We have developed and characterized a range of lead-germanate glasses that, when compared with other infrared transmitting high index glasses (such as tellurites) stand out for having the desirable properties of low phonon energy and high refractive index without compromising on fiber stability, due to the fact that they retain higher glass transition temperatures. Preliminary evaluation of fiber strength via a measurement of the bend radius (the radius at which the fiber breaks [49]) has yielded values of 21.5 ± 8.7 mm and 16.3 ± 5.9 mm for the TZNL and GPL5 bare fibers, respectively. The smaller bend radius for the germanate fiber indicates higher fiber strength. Further investigations will be conducted to thoroughly quantify the fiber strengths of tellurite and germanate fibers.

We find that in our glasses the partial replacement of PbO by La_2O_3 up to 5 mol% increases glass transition temperature without decreasing glass stability or refractive index.

We have also fabricated a suspended core microstructured fiber from one of these glasses and used it to measure a nonlinear refractive index that is comparable to that of tellurite and bismuth glasses. We believe this to be a significant result as it demonstrates both the fabrication of a small core microstructured fiber and showcases the high nonlinearity of the material ($n_2 = 56 \pm 6 \times 10^{-20}$ m^2W^{-1}). The extrusion based fabrication technique is also readily expandable and thus this fiber represents a first step in the potential fabrication of more complex geometries, such as those required for dispersion engineered fibers.

Therefore we believe these new lead-germanate glasses are promising candidates for many

#192254 - $15.00 USD Received 17 Jun 2013; revised 18 Aug 2013; accepted 18 Aug 2013; published 27 Aug 2013

infrared optical fiber applications, especially those requiring high nonlinearity and/or high gain.

Acknowledgments

We acknowledge the Asian Office of Aerospace R&D (AOARD 104120) and the German Academic Exchange Service (DAAD) and the Group of Eight (Go8) universities and ARC support (DP110104247) for funding this work. This work was performed in part at the OptoFab node of the Australian National Fabrication Facility utilizing Commonwealth and SA State Government funding. We wish to thank the following co-workers at the University of Adelaide for their help with this research: Katarina Markulic, Rachel Moore and Kenton Knight for glass fabrication; Roger Moore and Alastair Dowler for fiber fabrication; Robin Pötter and Kenton Knight for IR transmission measurements; and Sean Manning for the nonlinear index measurement of the TZNL glass. We also thank Sebastian Krolikowski at the University of Erlangen-Nürnberg for his help with glass fabrication and DSC measurements and Sabine Brungs for thermal analyses, and Christian Mühlig at the Institute for Photonic Technology in Jena for the absolute absorption measurements. D. Manzani thanks FAPESP (Fundação de Amparo à Pesquisa do Estado de São Paulo). T. Monro acknowledges the support of an Australian Research Council Federation Fellowship.